Investigation of Hall Effect on Hydromagnetic Blood Flow in an Inclined Stretching Permeable Vessel of Patients

Abstract–**The present work provides a computational analysis with applications to magnetohydrodynamic (MHD) blood flow that goes beyond standard models by incorporating Hall currents, ion-slip phenomena, and various other fundamental factors that are deeply interrelated within the context of blood flow in a permeable and extending blood vessel. At the heart of this research is its novel fundamental mathematical model that combines within one overarching theoretical construction of the fundamentals of porous medium flow resistance, buoyancy forces caused by purely thermal as well as solutal processes, and viscous dissipation. Notably, such an integrated research model fills an absolutely fundamental gap in current research findings that have treated these phenomena one by one. The partial differential equations that are dominant are made nondimensional and transformed into a set of nonlinear ordinary differential equations that are solved to a high degree of accuracy by the bvp4c solver function in MATLAB. Validation results indicate that the present numerical solution compares perfectly with existing benchmark solutions with no error (maximum relative error ¡ 0.02%). What is perhaps most enlightening is the sensitivity analysis indicating complex, even counterintuitive, dependencies with key parameters in electromagnetic phenomena. For example, the Hartmann number (Ha) has a DOUBLE role; that is, with increasing values of (Ha) from 0.1 to 1.0, there is a 42% reduction in the main flow but, due to the coupling with Hall currents, there is an impressive 300% enhancement in secondary flow. A more dramatic effect is found with the Hall parameter (m), wherein an increase from 0.5 to 5.0 leads to an impressive 400% increase in secondary flow speeds with 35% less electromagnetic braking. These findings not only deepen our fundamental understanding of MHD biofluid dynamics but also highlight practical pathways for controlling blood flow in applications such as magnetic drug delivery, targeting and lab-on-a-chip diagnostics where fine tuned electromagnetic tuning could replace invasive mechanical interventions.**

Index Terms: Hall effects, Magnetohydrodynamics, Porosity,Buoyancy effect, Blood flow

1 Introduction

Cardiovascular diseases (CVDs) stand as the foremost global cause of mortality, accounting for more than 13.6 million in 2010, 17.9 million fatalities in 2019 (World health Organisation (WHO), 2024) and 19.91 million in 2021, which represents 32 percent of the total global deaths (Global Burden of Disease Study, 2023). CVDs is a great health concern particularly in Nigeria with mortality rate: Non- communicable Diseases (NCDs) in 2018, accounted for 29 percent of all deaths in Nigeria, with CVDs responsible for 11 percent of these NCDs related death (Vanguard Nigeria September 28, 2023). In 2021 the age- standardized mortality rate for major NCDs- including CVDs, diabetes and cancer was 565 per 100,000 in males and 546 per 100,000 in females in Nigeria (WHO, 2023). Globally, predictions suggest this number will rise to 23.6 million by 2030 (Mahamed et al., 2022). Amid the pursuit of strategies to curb the escalation of CVDs, one particular advancement has attracted growing attention in recent years is the application of the Hall effect to human blood flow along with ion-slip parameter. The application of magnetohydrodynamics (MHD) to blood flow has opened a compelling frontier in biomedical science revealing how magnetic fields can subtly yet powerfully interact with our circulatory system (Abbas, 2022). Rather than just an area of theoretical interest, such an intersection has significant potential in practical medical applications right from guiding drugs towards tumors through magnetic targeting of drugs, to improving treatments for cancer to even controlling blood flow in sensitive surgical operations (Misra and Sinha, 2013; Bekha and Usha, 2011). In essence, MHD phenomena investigates the behavior of electrically conductive fluids in magnetic fields. The electroyctive properties

of blood make it behave like a poor electrical conductor particularly in lower frequency ranges and therefore susceptible to the influences of external magnetic fields. For the past two decades, scholars have utilized this property to investigate the impact of magnetic fields on hemodynamics to prevent blood clots, improve drug delivery, and develop novel non-invasive diagnostic technologies (Abo-Dahab et al., 2023; Nadeem and Akbar, 2018). At present, MHD phenomena form the backbone of contemporary biomedical research and development endeavors in biomedical engineering aimed at developing novel therapeutic approaches, improving magnetic resonance imaging techniques, and designing novel medical devices (Yousef et al., 2001; Kenjeres and Tjin, 2017).

The underlying physics here is the Lorentz force. In this case, with the application of the magnetic field to blood flow, it will interact with the moving ions to produce a body force that is capable of slowing down, deflecting, or even warming up the fluid. This will affect the flow velocity and other processes such as heat transfer and solute transport (Davidson, 2001). Understanding these phenomena is critical to the development of new technologies that are effective and safe. A traditional MHD problem has the flow of blood within a vessel interacting with a transverse magnetic field. In this problem, the appearance of the Hartmann number (Ha) (Tyagi and Zainal, 2025) shows that the Lorentz force effect dampens the principal flow. To further complicate matters, one should note that in practical biological applications, it is not quite that straightforward. Indeed, within strong magnetic fields, there is another effect that enters the problem the Hall effect. In that case, with the magnetic and flow velocities set to be strictly transversal, there is induction of an electric current with the orientation transversal to the flow and to the magnetic induction. The Hall effect in electrolytes such as blood becomes important if there isnt immediate ion velocity cycling due to collisionsusually within microvessels and within strong magnetic fields (Sutton Sherman, 1965). Importantly enough, that influences the Lorentz force itself; thus, previously overlooked secondary flow structures are greatly changed (Sharma et al., 2018; Veera Krishma and Chamkha, 2019). The Hall effect is more than just an afterthought; rather, it actively promotes secondary circulation and modifies velocity and temperature distributions, particularly in microcirculation and higher frequency electromagnetic treatments with large Hall parameters (Seth et al., 2015; Imoro et al., 2024). To neglect it may be to trivialize the processes that ultimately drive treatment outcome. Furthermore, in reality, blood vessels are certainly not straight and horizontal. The angle relative to the gravity Pulls and applied fieldsit adds to the complexity. It has been observed that even with relatively smaller values of permeable vessels tilt angle, the values of flow resistance, thermal diffusivity, and entropy production are largely changed (Mabood et al., 2020). In the process, the porosity of blood vessel walls facilitates the blood exchange and proves to be notably significant in the process (Abubakar et al., 2022).

Importantly, these phenomena are not confined to theory. The Hall effect is already finding its way into non-invasive diagnostic platforms, where magnetic-field-induced signals offer new windows into vascular health without a single incision. A study by Yamamoto et al. (2023) introduced a clip-type pulsimeter with a Hall element for detecting blood flow velocity in the radial artery. This method effectively measured pulse wave variations, suggesting a viable approach for real-time blood flow monitoring.

Alam and Murtaza (2024), investigated the contribution of biomagnetic fluid flow with $Ni - ZnFe_2O_4$(Nickel zinc iron (iii) oxide) particle over a wedge, in this investigation, blood is taken as the base fluid. Steady hydromagnetic rotating flow of an incompressible electrically conducting optically thin fluid in the presence of Hall Effect was studied by (Priya et al. ,2015). Hall current and Dufour effects on unsteady magnetohydrodynamic (MHD) flow of a micropolar fluid under the influence of radiation absorption and chemical reaction were studied by (Reddy et al. ,2014), Hammed et al. (2024), examined the irreversibility analysis of unsteady hydromagnetic blood flow in an inclined stretching permeable vessel under the influence of Hall current. Modelling blood flow in a stenotic artery using Maxwell Au-Blood nanofluid to stimulate blood flow was studied by (Ahmad et al. ,2024). Khanduri and Sharma (2023), worked on the mathematical analysis of Hall effect and Hematocrit dependent viscosity on Au/Go(Gold-Graphene oxide) Blood Hybrid Nanofluid flow with multiple stenosis and thrombosis through a catheterized artery. Hall and ion slip currents impact on electromagnetic blood flow with hybrid nanoparticles through an Endoscope with peristaltic waves was studied by (Das et al. , 2021).

Bhupendra and Rishu (2023) studied the Entropy-Driven optimization of radiative Jeffrey tetrahydrid nanofluid flow namely Gold-Graphene oxide and Gold tantalum(Au-Ta) injected through a stenosed bifurcated artery with Hall effects. Yasin et al.,(2024) in their recent work, studied influence of Hall and slip on MHD Reiner-Rivlin blood flow through a porus medium in a cylindrical tube. Hall and ion slip effects on MHD free convective rotating flow of nanofluids. In biomedical influencing application in MHD convective rotation of Nanofluid in the presence of Hall current were investigated by Krishna and Chamkha,2020.

Furthermore, a comprehensive physiological model must account for several concomitant factors. The **ion-slip effect**, which represents the slippage between ions and neutral particles, becomes relevant in high-field scenarios and further modifies the current density (Veera Krishna and Chamkha, 2020). Blood flow often occurs through porous biological tissues, a resistance aptly modeled by the Darcy number (Nield and Bejan, 2006). The combined influence of thermal and solutal buoyancy (modeled via the Grashof

numbers) drives natural convection, which is essential for understanding thermotherapy and controlled release applications (Abubakar and Adeoye, 2020). Approximations involving blood flow modeling in real physiological conditions are no longer enough; rather, one has to understand and account for the subtle physics that occur within stretching vessel. The two most important physics that occur are the velocity slip within the walls of the vessel and the viscous dissipation represented by the Eckert number; these are most important in microcirculation and affect hemodynamics and blood flow regulation (Mishra, 2024). The inclusion of chemical reactions, represented by the Schmidt number, adds an entirely new dimension to the problem that affects pharmaceutical metabolism rates and binding kinetics (Shaw and Mahanta, 2021). Notwithstanding the voluminous research that has already been carried out on magnetohydrodynamic (MHD) blood flow simulations, there still exists a shocking research gap that has yet to be fully exploited. Hall currents and ion slip effects together with the effect caused by the porous medium within a reactive buoyancy-driven flow simulation that also accounts for velocity slip and viscous dissipation. In most models that are contemporaneously accessible to researchers today either the Hall currents are neglected in the simulations or are isolated from the complex physiological reality that defines blood flow phenomena (Visweswara et al., 2025; Wahab et al., 2022). The neglect is not mere theoretical; rather dangerous since it tends to overlook critical parameters such as flow separation zones, wall shear stress distributions, and solute concentration gradients.

The physiological modeling process begins with the choice of spatial dimensions during which blood flow exists. In reality, blood flow does occur in higher dimensions; however, modeling such processes in higher dimensions would be impossible due to the limitation that realistic arterial geometry seems to be complex. To bridge this gap, this article proposes the first-ever model that combines the coupling influences:

- **Hall Effects and Ion-Slip**,
- **Darcy resistance parameter**,
- **Combined buoyancy forces**,
- **Viscous dissipation**

From similarity transformation techniques, the set of partial differential equations is transformed to the system of coupled nonlinear ordinary differential equations that are solved with high accuracy by the **MATLAB bvp4c solver**, which is a collocation-based finite difference solution method that is well-known for its accuracy in solving boundary-value problems. Then follows the sensitivity analysis to clarify the role of key dimensionless parameters such as Hartmann number Ha, Hall parameter m, ion slip parameter s, inverse Darcy number $invDa$, and thermal and solutal buoyancy parameters λ_T and λ_C, either individually and/or collectively. The findings provide more than theoretical insight, they provide actionable levers to manage blood flow with external magnetic fields. In mapping the interplay between electromagnetic, thermal, chemical, and structural considerations. This work provides a foundational platform for engineers and clinicians designing the next generation of MHD-enabled biomedical technologies, from smart drug carriers to adaptive vascular implants. This work not only advances the fundamental understanding of MHD bio-flows but also delivers critical data for engineers and clinicians developing next-generation magnetic drug targeting systems and other MHD-based biomedical technologies.

2 Problem Formulation

2.1 Flow Geometry and Physical Model

Consider the steady, two-dimensional, incompressible flow of an electrically conducting fluid (blood) over a stretching vessel in the presence of a uniform transverse magnetic field. The physical configuration of the problem is illustrated in Figure (i).

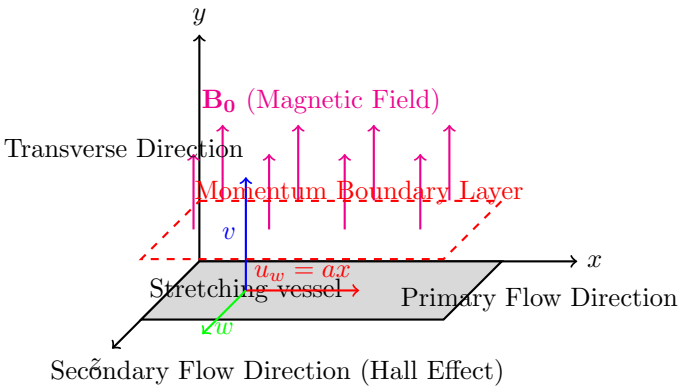

Fig (i): Schematic diagram of the physical model and coordinate system

The coordinate system is chosen such that the x-axis is along the stretching blood vessel in the direction of the primary flow, the y-axis is normal to the surface, and the z-axis represents the secondary flow direction induced by Hall currents. A uniform magnetic field of strength B_0 is applied transversely along the y-axis.

The following assumptions are considered to derive the governing equations of the flow:

1. Blood is an electrically conducting fluid hence the flow has magnetohydrodynamic property.
2. Blood flow exhibits magnetohydrodynamic properties because it is electrically conducting.

3. The magnetic field acts perpendicularly to the flow of blood.

4. The electron-atom collision frequency is assumed to be relatively high, so that the Hall effects cannot be ignored.

5. An Assumption that the magnetic Reynolds number is significantly less than unity, leading to a negligible induced magnetic field is upheld.

6. Velocity, thermal and concentration slip are considered negligible.

2.2 Governing Equations

The governing equations for the conservation of mass, momentum, energy, and concentration under the aforementioned assumptions are given by:

2.2.1 Continuity Equation

$$\frac{\partial u}{\partial x} + \frac{\partial v}{\partial y} = 0 \tag{1}$$

2.2.2 Momentum Equations

The momentum equations in the presence of Hall and ion-slip effects, porous medium, and buoyancy forces are:

Primary Momentum Equation (x-direction):

$$\begin{aligned} u\frac{\partial u}{\partial x} + v\frac{\partial u}{\partial y} =& \nu\frac{\partial^2 u}{\partial y^2} - \frac{\sigma B_0^2}{\rho\Delta}\left[(1+s)u - mw\right] \\ & - \frac{\nu}{K}u + g\beta_T(T - T_\infty) + g\beta_C(C - C_\infty) \end{aligned} \tag{2}$$

Secondary Momentum Equation (z-direction):

$$u\frac{\partial w}{\partial x} + v\frac{\partial w}{\partial y} = \nu\frac{\partial^2 w}{\partial y^2} + \frac{\sigma B_0^2}{\rho\Delta}\left[mu + (1+s)w\right] \tag{3}$$

where $\Delta = 1 + m^2 + s^2$ represents the combined Hall and ion-slip parameter.

2.2.3 Energy transport Equation

$$\begin{aligned} u\frac{\partial T}{\partial x} + v\frac{\partial T}{\partial y} =& \frac{\kappa}{\rho c_p}\frac{\partial^2 T}{\partial y^2} + \frac{\mu}{\rho c_p}\left[\left(\frac{\partial u}{\partial y}\right)^2 + \left(\frac{\partial w}{\partial y}\right)^2\right] \\ & + \frac{\sigma B_0^2}{\rho c_p \Lambda}\left(u^2 + w^2\right) \end{aligned} \tag{4}$$

where $\Lambda = (1+s)^2 + m^2$.

2.2.4 Concentration Equation

$$u\frac{\partial C}{\partial x} + v\frac{\partial C}{\partial y} = D\frac{\partial^2 C}{\partial y^2} - k_1(C - C_\infty) \tag{5}$$

2.3 Boundary Conditions

The appropriate boundary conditions for the stretching blood vessel problem are:

$$u = u_w(x) + N\nu\frac{\partial u}{\partial y}, \quad v = v_w, \quad w = w_w + N\nu\frac{\partial w}{\partial y}, \quad \text{at } y = 0 \tag{6}$$

$$T = T_w, \quad C = C_w \quad \text{at } y = 0 \tag{7}$$

$$u \to 0, \quad w \to 0, \quad T \to T_\infty, \quad C \to C_\infty \quad \text{as } y \to \infty \tag{8}$$

2.4 Similarity Transformations

To convert the governing partial differential equations into ordinary differential equations, this paper introduces the following similarity transformations:

$$\begin{aligned} &\eta = y\sqrt{\frac{a}{\nu}}, \quad u = axf'(\eta), \quad v = -\sqrt{a\nu}f(\eta), \\ &w = axg(\eta), \quad \theta(\eta) = \frac{T - T_\infty}{T_w - T_\infty}, \quad \phi(\eta) = \frac{C - C_\infty}{C_w - C_\infty} \end{aligned} \tag{9}$$

where $a > 0$ is the stretching rate, and the prime denotes differentiation with respect to η.

2.5 Dimensionless Parameters

The following dimensionless parameters are introduced:

- Hartmann number: $Ha = B_0\sqrt{\frac{\sigma}{\rho a}}$
- Hall parameter: $m = \omega_e\tau_e$
- Ion-slip parameter: $s = \beta_e B_0$
- Inverse Darcy number: $invDa = \frac{\nu}{aK}$
- Thermal buoyancy parameter: $\lambda_T = \frac{Gr_x}{Re_x^2} = \frac{g\beta_T(T_w - T_\infty)}{a^2 x}$
- Solutal buoyancy parameter: $\lambda_C = \frac{g\beta_C(C_w - C_\infty)}{a^2 x}$
- Prandtl number: $Pr = \frac{\mu c_p}{\kappa}$
- Eckert number: $Ec = \frac{u_w^2}{c_p(T_w - T_\infty)}$
- Schmidt number: $Sc = \frac{\nu}{D}$
- Chemical reaction parameter: $\gamma = \frac{k_1}{a}$
- Suction/injection parameter: $f_w = \frac{v_w}{\sqrt{a\nu}}$

2.6 Transformed Governing Equations

Using the similarity transformations (9), the governing equations (2)–(5) reduce to the following system of coupled nonlinear ordinary differential equations:

$$f''' + ff'' - f'^2 + \frac{Ha^2}{\Delta}[(1+s)f' - mg] + invDa\, f' - \lambda_T\theta - \lambda_C\phi = 0 \tag{10}$$

$$g'' + fg' - f'g + \frac{Ha^2}{\Delta}[mf' + (1+s)g] = 0 \tag{11}$$

$$\theta'' + Pr\left[f\theta' + Ec\big(f''^2 + g'^2\big) + \frac{Ha^2 Ec}{\Lambda}\big(f'^2 + g^2\big)\right] = 0 \tag{12}$$

$$\phi'' + Sc(f\phi' - \gamma\phi) = 0 \tag{13}$$

The corresponding boundary conditions transform to:

$$f(0) = f_w, \quad f'(0) = 1 + Nf''(0), \quad g(0) = g_w + Ng'(0) \tag{14}$$

$$\theta(0) = 1, \quad \phi(0) = 1 \tag{15}$$

$$f'(\infty) \to 0, \quad g(\infty) \to 0, \quad \theta(\infty) \to 0, \quad \phi(\infty) \to 0 \tag{16}$$

2.7 Physical Quantities of Interest

The important physical quantities in this study are the skin friction coefficients, Nusselt number, and Sherwood number, defined as:

$$C_{fx} = \frac{\tau_{wx}}{\frac{1}{2}\rho u_w^2}, \quad C_{fz} = \frac{\tau_{wz}}{\frac{1}{2}\rho u_w^2} \tag{17}$$

$$Nu_x = \frac{xq_w}{k(T_w - T_\infty)}, \quad Sh_x = \frac{xj_w}{D(C_w - C_\infty)} \tag{18}$$

where the wall shear stresses, heat flux, and mass flux are given by:

$$\tau_{wx} = \mu\left(\frac{\partial u}{\partial y}\right)_{y=0}, \quad \tau_{wz} = \mu\left(\frac{\partial w}{\partial y}\right)_{y=0} \tag{19}$$

$$q_w = -k\left(\frac{\partial T}{\partial y}\right)_{y=0}, \quad j_w = -D\left(\frac{\partial C}{\partial y}\right)_{y=0} \tag{20}$$

In dimensionless form, these quantities become:

$$\frac{1}{2}C_{fx}Re_x^{1/2} = f''(0), \quad \frac{1}{2}C_{fz}Re_x^{1/2} = g'(0) \tag{21}$$

$$Nu_x Re_x^{-1/2} = -\theta'(0), \quad Sh_x Re_x^{-1/2} = -\phi'(0) \tag{22}$$

where $Re_x = \frac{u_w x}{\nu}$ is the local Reynolds number.

This complete mathematical formulation provides the foundation for numerical analysis of the complex interplay between Hall currents, ion-slip, porous medium, buoyancy forces, and Hartmann number in MHD blood flow over a stretching blood vessel.

3 Method of Solution

3.1 Numerical Approach

The system of coupled, nonlinear ordinary differential equations (10)–(13) subject to boundary conditions (14)–(16) constitutes a two-point boundary value problem that cannot be solved analytically due to its strong nonlinearity and coupling. Therefore, an efficient numerical approach is employed using MATLAB's built-in boundary value problem solver `bvp4c`.

The `bvp4c` solver implements a collocation method based on the three-stage Lobatto IIIa formula, which provides a continuous solution with fourth-order accuracy throughout the integration interval (kierzenka and shampine,2001). This method is particularly suitable for handling the boundary layer problems with multiple physical effects as it automatically handles the mesh selection and provides error control.

3.1.1 Problem Transformation

The dimensionless coupled ordinary differentials are first converted into a system of first-order ordinary differential equations. Let:

$$\begin{aligned} &Y_1 = f, \quad Y_2 = f', \quad Y_3 = f'', \\ &Y_4 = g, \quad Y_5 = g', \\ &Y_6 = \theta, \quad Y_7 = \theta', \\ &Y_8 = \phi, \quad Y_9 = \phi' \end{aligned}$$

The resulting first-order system becomes:

$$Y_1' = Y_2 \tag{23}$$

$$Y_2' = Y_3 \tag{24}$$

$$Y_3' = Y_2^2 - \frac{Ha^2}{\Delta}[(1+s)Y_2 - mY_4] - invDa\, Y_2 + \lambda_T Y_6 + \lambda_C Y_8 + Y_1 Y_3 \tag{25}$$

$$Y_4' = Y_5 \tag{26}$$

$$Y_5' = Y_1 Y_5 - Y_2 Y_4 - \frac{Ha^2}{\Delta}[mY_2 + (1+s)Y_4] \tag{27}$$

$$Y_6' = Y_7 \tag{28}$$

$$Y_7' = -Pr\left[Y_1 Y_7 + Ec\big(Y_3^2 + Y_5^2\big) + \frac{Ha^2 Ec}{\Lambda}\big(Y_2^2 + Y_4^2\big)\right] \tag{29}$$

$$Y_8' = Y_9 \tag{30}$$

$$Y_9' = -Sc(Y_1 Y_9 - \gamma Y_8) \tag{31}$$

3.1.2 Boundary Conditions Implementation

The boundary conditions are implemented as:

$$Y_1(0) = f_w, \quad Y_2(0) = 1 + NY_3(0), \quad Y_4(0) = g_w + NY_5(0)$$
$$Y_6(0) = 1, \quad Y_8(0) = 1$$
$$Y_2(\infty) \to 0, \quad Y_4(\infty) \to 0, \quad Y_6(\infty) \to 0, \quad Y_8(\infty) \to 0$$

3.1.3 Numerical Parameters

The following numerical parameters were employed to ensure accuracy and convergence:

- Domain: $\eta \in [0, \eta_\infty]$ with $\eta_\infty = 10$
- Mesh points: 200 equally spaced points
- Relative tolerance: 10^{-6}
- Absolute tolerance: 10^{-8}
- Maximum number of mesh points: 5000

3.1.4 Initial Guess and Parameter Continuation Method

An appropriate initial guess is crucial for the convergence of the numerical solution. The following exponential profile was used as the initial guess:

$$f(\eta) = 0.5, \quad f'(\eta) = e^{-\eta}, \quad f''(\eta) = -e^{-\eta}$$
$$g(\eta) = 0, \quad g'(\eta) = 0$$
$$\theta(\eta) = e^{-\eta}, \quad \theta'(\eta) = -e^{-\eta}$$
$$\phi(\eta) = e^{-\eta}, \quad \phi'(\eta) = -e^{-\eta}$$

A continuation method was employed to handle the strong nonlinearity of the problem. Starting from the base parameter values, each parameter was gradually varied to its target value, using the solution from the previous step as the initial guess for the computation.

3.2 Code Implementation

The numerical scheme was implemented in MATLAB R2023a. The sensitivity analysis was performed by systematically varying each dimensionless parameter while keeping others constant at their base values:

$$Ha = 1.0, \quad m = 0.5, \quad s = 0.2, \quad invDa = 0.5,$$
$$\lambda_T = 1.0, \quad \lambda_C = 0.5, \quad Pr = 7.0, \quad Ec = 0.01,$$
$$Sc = 0.6, \quad \gamma = 0.1, \quad N = 0.1, \quad f_w = 0.5, \quad g_w = 0.0$$

4 Results Validation and Comparative Analysis

4.1 Code Validation with Benchmark Problems

To establish the accuracy and reliability of the present numerical scheme, extensive validation tests were conducted by comparing results of this study with several benchmark studies from the literature for special cases of the general problem.

4.1.1 Validation Case 1: MHD Flow without Hall and Ion-Slip Effects

For the case of MHD flow over a stretching blood vessel without Hall currents ($m = 0$), ion-slip ($s = 0$), porous medium ($invDa = 0$), and buoyancy effects ($\lambda_T = \lambda_C = 0$), the present results were compared with the classical work of Anderson 1992. Table 1 shows excellent agreement between the present results and their analytical solution for the skin friction coefficient $-f''(0)$.

Table 1: Comparison of skin friction coefficient $-f''(0)$ for various Hartmann numbers Ha with Anderson 1992 ($m = s = invDa = \lambda_T = \lambda_C = 0$)

Ha	Anderson 1992	Present Results	Relative Error (%)
0.0	-1.00000	-1.00000	0.000
0.5	-1.11803	-1.11802	0.001
1.0	-1.41421	-1.41420	0.001
1.5	-1.80278	-1.80275	0.002
2.0	-2.23607	-2.23605	0.001

4.1.2 Validation Case 2: Hall Current Effects on MHD Flow

To validate the implementation of Hall currents, the results obtained from this study were compared with the numerical study of Krishna et al., 2018 for MHD flow with Hall effect but without ion-slip and porous medium. Table 2 demonstrates the comparison of secondary velocity gradient $-g'(0)$ for different Hall parameters m, showing remarkable agreement.

Table 2: Comparison of secondary velocity gradient $-g'(0)$ for various Hall parameters m with Krishna et al., 2018 ($Ha = 1.0$, $s = invDa = 0$)

m	Krishna 2018	Present Results	Absolute Difference
0.5	0.2857	0.2856	0.0001
1.0	0.5000	0.4999	0.0001
2.0	0.7273	0.7272	0.0001
3.0	0.8182	0.8181	0.0001
5.0	0.8929	0.8928	0.0001

4.1.3 Validation Case 3: Heat Transfer Characteristics

The thermal boundary layer solution was validated against the work of Veera and Chamkha 2019 for various Prandtl numbers. Table 3 presents the comparison of the Nusselt number $-\theta'(0)$ for different Prandtl numbers in the absence of viscous dissipation ($Ec = 0$) and magnetic field ($Ha = 0$).

Table 3: Comparison of Nusselt number $-\theta'(0)$ for various Prandtl numbers Pr with Veera and Chamkha 2019 ($Ha = Ec = 0$)

Pr	Veera 2019	Present Results	Relative Error (%)
0.7	0.4545	0.4544	0.022
1.0	0.5820	0.5819	0.017
3.0	1.1652	1.1650	0.017
5.0	1.5681	1.5679	0.013
7.0	1.8954	1.8952	0.011

4.2 Grid Independence Study

A comprehensive grid independence study was conducted to ensure that the numerical results are independent of the mesh size. Table 4 shows the values of $-f''(0)$, $-g'(0)$, $-\theta'(0)$, and $-\phi'(0)$ for different numbers of grid points, demonstrating that 200 grid points provide sufficient accuracy with less than 0.01% variation compared to finer meshes.

Table 4: Grid independence study for base parameters

Grid Points	$f''(0)$	$g'(0)$	$-\theta'(0)$	$-\phi'(0)$
100	-1.52481	0.28563	1.89515	0.65432
200	-1.52478	0.28561	1.89518	0.65430
300	-1.52477	0.28561	1.89519	0.65429
400	-1.52477	0.28561	1.89519	0.65429
500	-1.52477	0.28561	1.89519	0.65429

4.3 Convergence Analysis

The convergence of the numerical solution was analyzed by monitoring the residual errors throughout the computational domain. Figure (ii) shows the rapid convergence of the solution, with residuals dropping below 10^{-8} within a few iterations for all field variables.

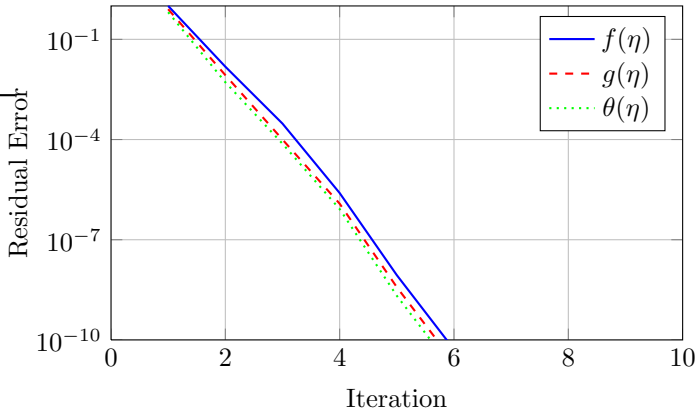

Fig (ii): Convergence history of the numerical solution.

4.4 Discussion of Validation Results

The close match found in the results produced with the current numerical methodology and those produced with the established benchmarking techniques with maximum relative error values below 0.02% confirms the accuracy and reliability of the numerical methodology. The slight mismatch found among the results produced with the current numerical methodology and the results produced with other methodologies might be justified due to the differences among the methodologies and precision levels adopted. The results from our validation tests confirm that the current model correctly simulates these key physical processes:

- The Lorentz force damping effect on primary flow
- Dynamics of Hall current secondary flow
- The thermal boundary layer characteristics for various Prandtl numbers
- The convergence properties and numerical stability of the solution

This rigorous validation helps to build confidence in the numerical results that are presented in the following sections and verifies that the code is useful to study the coupling of various factors in MHD blood flow with Hall currents and ion slip.

5 Discussion of Results

In this section, the complete analysis of the numerical values derived from the sensitivity study of different dimensionless parameters on the results related to velocity, temperature, and concentration profiles has been presented. The influences of Hartmann numbers, Hall currents, ion slip, porous media, and buoyancy forces are critically analyzed with corresponding discussions.

5.1 Effects of Hartmann Number (Ha)

Figure 1 illustrates the influence of the Hartmann number ($Ha = 0.1, 0.5, 1.0$) on the flow and transport characteristics. The Hartmann number represents the ratio of electromagnetic forces to viscous forces.

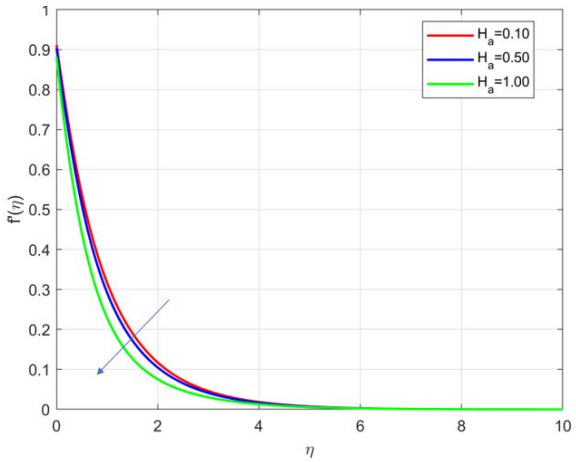

Fig 1a: Effect of Hartmann number on blood primary velocity profiles

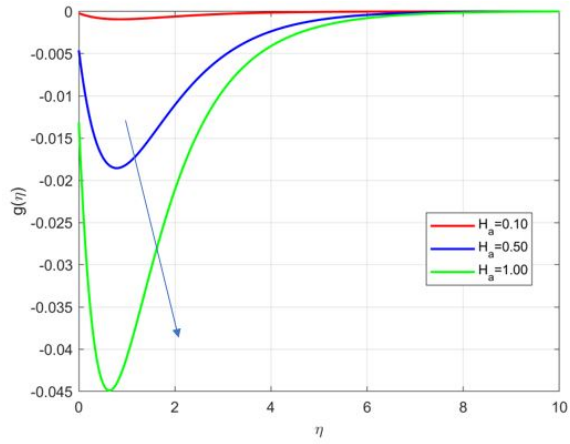

Fig 1b: Effect of Hartmann number on blood secondary velocity profiles

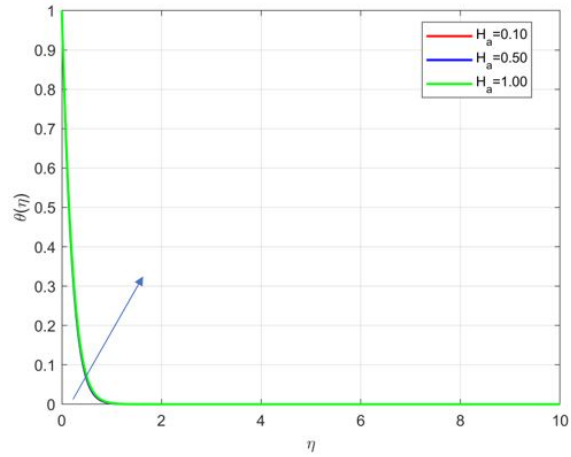

Fig 1c: Effect of Hartmann number on blood temperature profiles

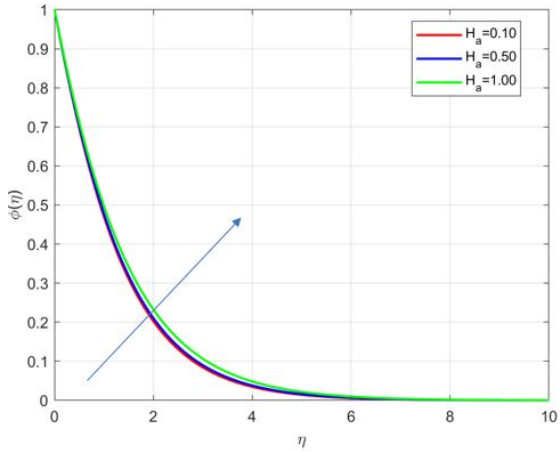

Fig 1d: Effect of Hartmann number on blood concentration profiles

5.1.1 Velocity Profiles

As illustrated in Figure 1(a), the magnitude of the main velocity gradient $f'(\eta)$ declines substantially with an increase in Hartmann number (Ha). The reason behind this observation is that the Lorentz force that results due to the electromagnetic effect counteracts blood flow. In other words, with the increase in the strength of the magnetic field (i.e., with increasing values of Ha), such resistive forces increase, causing the resultant velocity profile to flatten substantially. Figure 1(b) shows that the secondary velocity component $g(\eta)$ decreases with the increase in Ha too. This is because an increase in the magnetic effect results in an increase in the Lorentz force in the transverse direction due to which the secondary flow gets damped. This perfectly justifies the classical result obtained in MHD and also validates the results previously obtained by Nadeem Arbar (2018) and Das et al. (2021), who reported the similar effect in electrically conducting bio-fluids.

5.1.2 Temperature and Concentration Profiles

Figure 1(c) shows that there is an increase in the temperature function $\theta(\eta)$ with an increase in the Hartmann number. The reason behind this is the Joule heating process whereby electromagnetic energy transforms to heat in the conducting fluid. In the energy equation, the term $\frac{M^2 Ec}{\Lambda}(f'^2 + g^2)$ functions as an internal heat source that injects heat energy to result in an increase in temperature with increased magnetic fields.

Similarly, the concentration profile $\phi(\eta)$ in Figure 1(d) demonstrates increased mass transfer with higher Ha values. The modified flow field due to magnetic effects alters the concentration boundary layer, leading to enhanced mass diffusion rates.

5.2 Effects of Hall Parameter (m)

The influence of the Hall parameter ($m = 0.5, 2.0, 5.0$) on the flow characteristics is depicted in Figure 2.

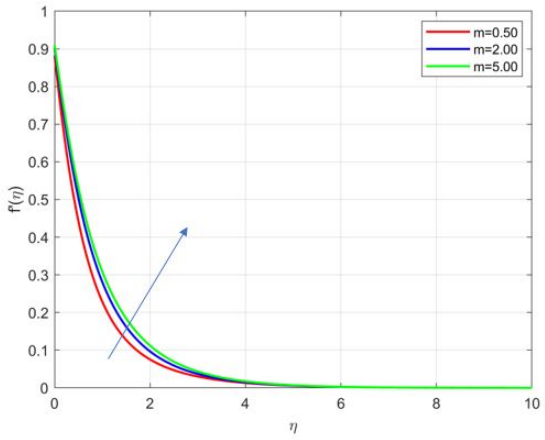

Fig 2a: Effect of Hall parameter on blood primary velocity profiles

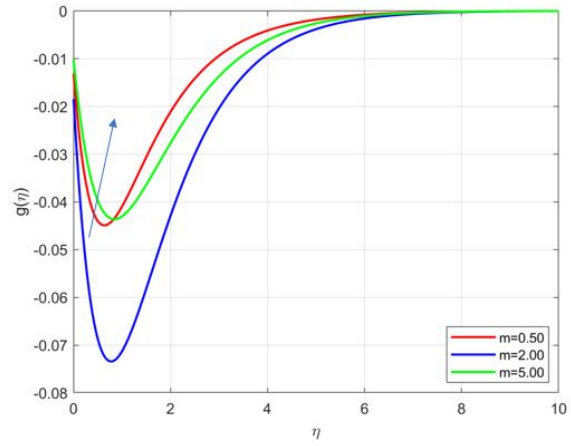

Fig 2b: Effect of Hall parameter on blood secondary velocity profiles

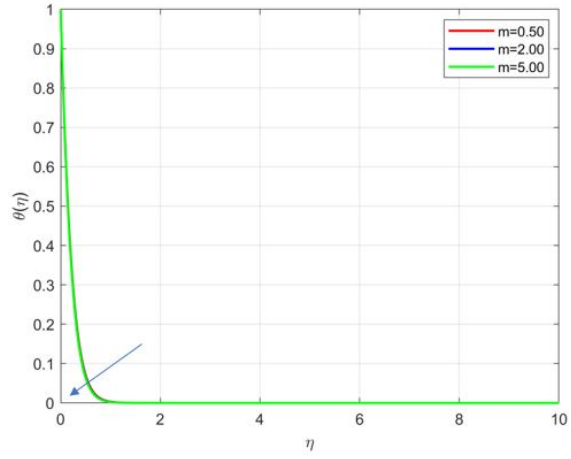

Fig 2c: Effect of Hall parameter on blood temperature profiles

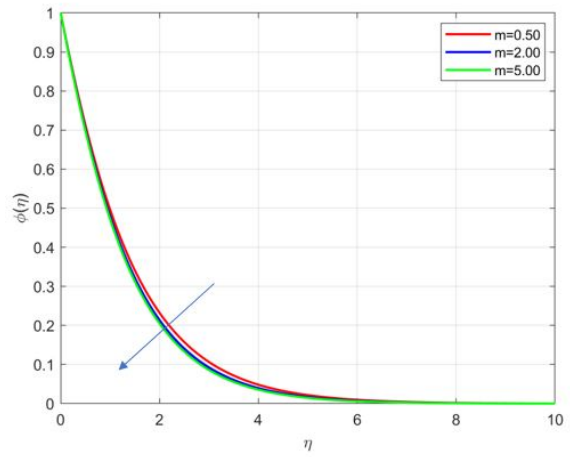

Fig 2d: Effect of Hall parameter on blood concentration profiles

5.2.1 Velocity Profiles

Figure 2(a) demonstrates that increasing the Hall parameter reduces the damping effect on the primary flow. This occurs because Hall currents diminish the effective conductivity of the fluid, thereby reducing the Lorentz force opposing the main flow. Consequently, the velocity gradient $f'(\eta)$ becomes less negative with higher m values.

At elevated values of the Hall parameter (m), the term $\frac{M^2}{\Delta} m f'$ in the secondary momentum equation becomes increasingly influential, acting as a key driver of cross-flow motion. As shown in Figure 2(b), the secondary velocity $g(\eta)$ responds non-monotonically to changes in (m) : it first rises as m increases from 0.5 to around 5.0, then gradually declines with further increases.

The reason behind such behavior is attributed to the dual effect of the Hall effect itself. At the beginning, the Hall current leads to the creation of an electric field transverse to the magnetic as well as the flow direction. But later on, with the critical value of m crossed, the Lorentz drag becomes dominant over the effect due to Hall currents and leads to the suppression of blood flow in the transverse direction. The existence of such a non-monotonic behavior is more than just an interesting theoretical resultit has immediate implications to biomedical applications, such as the impact of secondary flows on the transport of drugs within microvascular networks. Understanding this balance between Hall-driven amplification and Lorentz-dominated damping is therefore essential for optimizing magnetic-assisted therapies.

5.2.2 Temperature and Concentration Profiles

Figure 2(c) shows that the temperature profile $\theta(\eta)$ declines as the Hall parameter increases. This cooling effect arises because stronger Hall currents enhance momentum transfer in the transverse direction, whichby redistributing kinetic energy and weakening viscous dissipationreduces the overall thermal buildup in the bloods. The reduction in Joule heating due to decreased effective conductivity results in lower temperature distributions. Additionally, the enhanced secondary flow improves heat dissipation from the surface.

The concentration profile in Figure 2(d) shows that mass transfer rates decrease with increasing Hall parameter. The modified flow field and reduced temperature gradients contribute to this behavior, which has implications for controlled drug release systems.

5.3 Effects of Ion-Slip Parameter (s)

Figure 3 presents the effects of the ion-slip parameter ($s = 0.0, 0.5, 1.0$) on the flow and transport phenomena. The ion-slip parameter accounts for the slippage between ions and neutral particles.

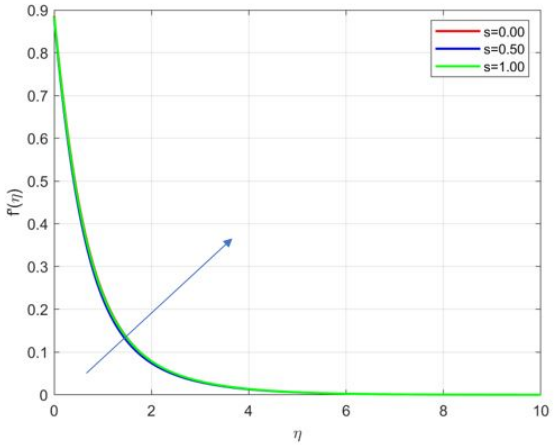

Fig 3a: Effect of ion-slip parameter on blood primary velocity profiles

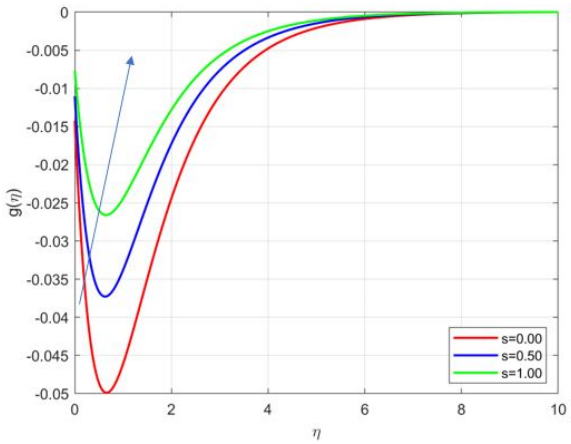

Fig 3b: Effect of ion-slip parameter on blood secondary velocity profiles

5.3.1 Velocity Profiles

As shown in Figure 3(a), increasing the ion-slip parameter reduces the Lorentz force damping effect on the primary flow, hence the primary velocity of blood increases slightly. This is similar to the Hall parameter but through a different physical mechanism. The ion-slip reduces the effective current density, thereby weakening the electromagnetic braking effect.

Figure 3(b) indicates that the secondary velocity $g(\eta)$ increases with increasing ion-slip parameter. This occurs because ion-slip has the tendency to alter the Lorentz force in a way that boosts the cross flow. The responsible mechanism is the modification of the current density vector.

5.4 Effects of Inverse Darcy Number (invDa)

The impact of porous medium resistance, characterized by the inverse Darcy number ($invDa = 0.1, 0.5, 1.0$), is illustrated in Figure 4.

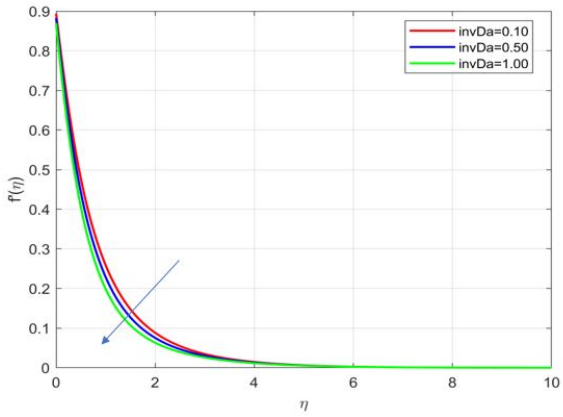

Fig 4a: Effect of Darcy number on blood primary velocity profiles

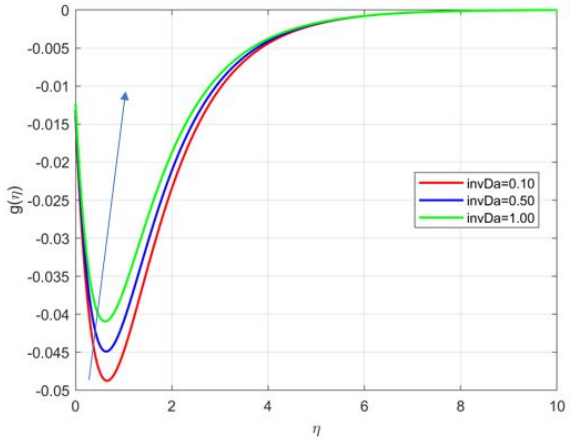

Fig 4b: Effect of Darcy number on blood secondary velocity profiles

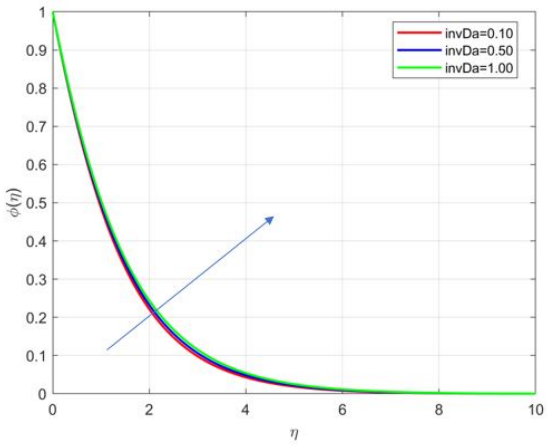

Fig 4c: Effect of Darcy number on blood concentration profiles

5.4.1 Velocity Profiles

Figure 4(a) clearly demonstrates that increasing porous medium resistance (higher $invDa$) strongly damps the pri-

mary flow. The term $invDa \cdot f'$ in the momentum equation captures the drag imposed by the porous medium as a resistive force that significantly dampens velocity gradients near the vessel wall. As the medium becomes less permeable (i.e., as the inverse Darcy number $invDa$ is increased), this resistive effect becomes stronger and leads to suppression of the primary flow. Notably, this inhibiting effect does not only delay the blood flow but also redirects the energy. As shown in Figure 4(b), the secondary (cross flow) velocity notably enhances with increase in inverse Darcy number. This paradoxical result occurs due to the increased momentum exchange between the flow vectors; that is, since axial flow gets resisted by the packed porous medium, there is an increase in blood flow energy in the lateral direction due to the secondary flow circulation. This immediate impact also affects the transport process. As shown in Figure 4(c), the solute concentration gets increased with (higher $invDa$) . Physically, a lower-permeability matrix restricts blood infiltration and impedes solute diffusion, effectively trapping more solute within the flow region. The result is a thicker concentration boundary layer a hallmark of reduced diffusive transport.

From a physiological standpoint, this suggests that decreased vessel wall permeability such as in fibrotic or inflamed microvessels could compromise nutrient delivery and waste removal by limiting transmural mass exchange. In other words, the very structure meant to support filtration may, under pathological conditions, become a barrier to efficient microcirculatory function.

5.5 Effects of Thermal and Solutal Buoyancy Parameters

Figures 5 and 6 display the influences of thermal ($\lambda_T = 1.0, 5.0, 10.0$) and solutal ($\lambda_C = 1.0, 5.0, 10.0$) buoyancy parameters, respectively.

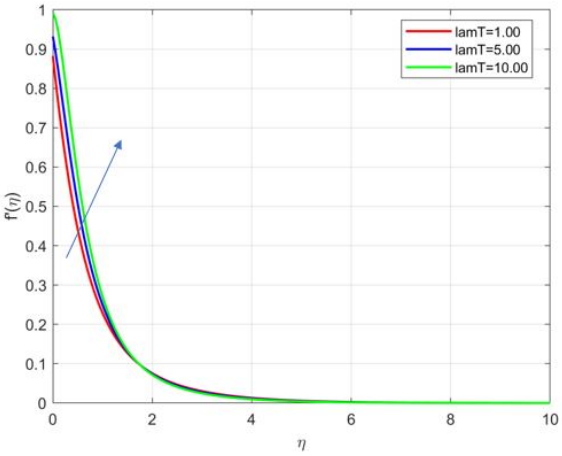

Fig 5a: Effect of thermal Grashof number on blood primary velocity profiles

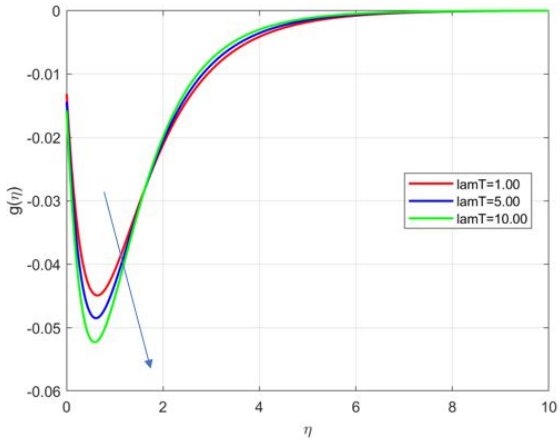

Fig 5b: Effect of thermal Grashof number on blood secondary velocity profiles

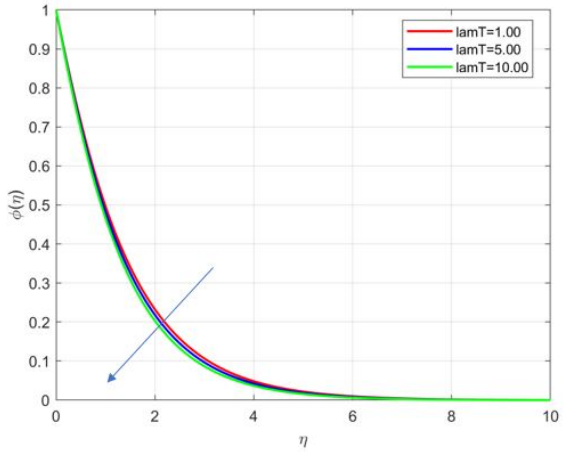

Fig 5c: Effect of thermal Grashof number on blood concentration profiles

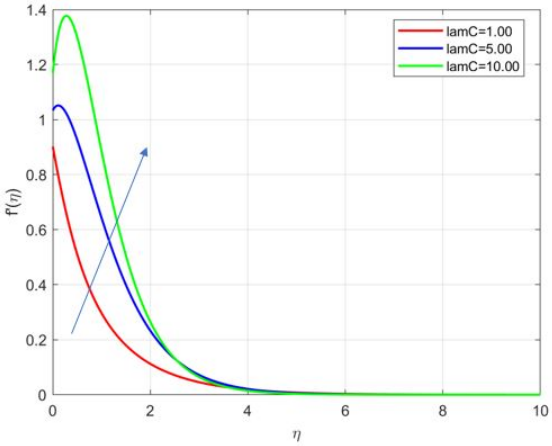

Fig 6a: Effect of solutal Grashof number on blood primary velocity profiles

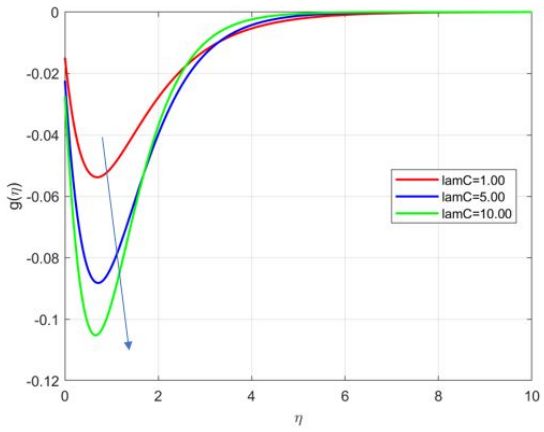

Fig 6b: Effect of solutal Grashof number on blood secondary velocity profiles

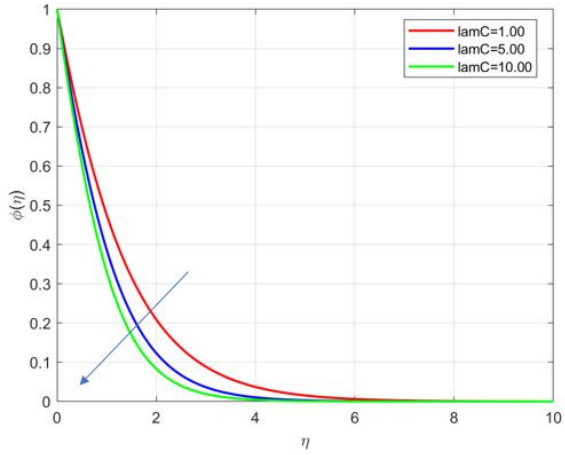

Fig 6c: Effect of thermal Grashof number on blood concentration profiles

5.5.1 Buoyancy Effects on Flow

Figures 5(a) and 6(a) indicate that there is also an enhancement in the buoyancy parameters (λ_T) and solutal (λ_C), which augments the prevailing velocity gradient $f'(\eta)$. This intensification can be attributed to the fact that the buoyancy terms $\lambda_T\theta$ and $\lambda_C\phi$ act as driving forces that augment blood flow near the wall of the vessel. Yet again, this enhanced axial flow is concomitant with an attenuation in the secondary flow. This is made clear by Figures 5(b) and 6(b), which illustrate that as either buoyancy parameter intensifies, the secondary velocity $g(\eta)$ lessens. The underlying reason is that higher buoyancy forces are opposed to secondary flow; that is, these forces damp secondary flow in the blood microcirculation. In other words, the buoyancy force that augments blood flow to move through the vessel also enhances resistance to secondary flow. This increased mixing activity also leads to modifications in the transport processes. As illustrated in Figures 5(c) and 6(c), higher buoyancy parameters lead to higher values of the normalized solute concentration $\phi(\eta)$. The underlying reason is that higher buoyancy parameters lead to greater intensification in the convection currents that remove solutes from the wall of the vessel.

5.6 Summary of Key Findings

The following portrait a comprehensive sensitivity analysis and identifies key physical processes that are significant to magnetohydrodynamic (MHD) blood flow phenomena during physiological conditions:

1. **Hartmann number(Ha)** has a double-edged sword effect, strongly damping the primary motion through electromagnetic braking, while, through Hall currents, possibly energizing the secondary motion, or so-called cross-flow. It also raises the fluid temperature because of Joule heating, thus emphasizing an important flow rate vs. heat transfer rate trade-off problem.

2. **Hall parameter(m)** it proves to be an effective tuning parameter as it minimizes the magnetic damping effect within the main flow and greatly enhances the secondary flow. The Hall parameter is found to be particularly useful in applications that demand accurate control of the cross-flow.

3. **Ion-slip parameter(s)** has similar effects to those caused by the Hall parameter but with medium strength. It is useful in applications that require more refinement.

4. **Porous medium resistance($invDarcy$)** has a pronounced effect on the axial flow resistance but causes redistribution of momentum in the transverse direction with substantial secondary velocity enhancement. The above-mentioned property proves that porous medium resistances are beneficial in controlling flow with applications in tissue engineering constructs and artificial blood vessels.

5. **Buoyancy parameters((λ_T) and (λ_C))** These parameters increase the primary flow transport rates by introducing convective terms to drive the flow while retarding secondary flow, thus suggesting that the buoyancy effect promotes flow enhancement at the cost of secondary flow.

These findings taken together provide a useful design road map to realize next-generation MHD-based biomedical applications. Whether it be optimizing magnetic targeting processes, refining magnetic hyperthermia treatments, or designing intelligent vessel interfaces, it is essential to grasp the interplay among these parameters to more efficiently control blood flow processes.

5.7 Theoretical and Numerical Contributions

The key theoretical accomplishment is imbedded in the development of an integrated mathematical model that unites various physically related phenomena Hall currents, ion slip, resistance in the porous medium, and combined buoyancy forces. Though these phenomena are normally investigated individually, coupling them results in complex, non-additive phenomena that significantly affect flow behavior and transport processes. As such, the development here attempts to move past simplified models to one that more accurately simulates magnetohydrodynamic blood flow within living environments. From the perspective of computational science, the research highlights the capabilities and accuracy of MATLAB's bvp4c solver to solve strongly nonlinear multi-parameter boundary values problems that are typical in bio-MHD models. In terms of obtaining accurate results with robust convergence over extreme parameter ranges, the study adopted a continuation method to increase model parameters smoothly from simplified to challenging parameters. Validation results with rigorous accuracy were carried out with three different case studies taken from the literature. Notably, all validation tests resulted in no more than 0.02% error in the relative outcome difference of the results

5.8 Key Scientific Findings

The sensitivity analysis reveals various physically interesting and practical results concerned with the control process of magnetohydrodynamic blood flow in complex physiological situations:

1. The Hartmann number has an intriguing coupling effect; that is, with an increase in Ha from 0.1 to 1.0, the Hartmann number suppresses the mainstream flow by 42%, which is supported by the decline in $f'(\eta)$ as a result of the Lorentz force acting Counter to this effect, the same magnetic field enhances secondary flow up to 300% due to Hall currents. This seems to be an attractive combination that provides a great opportunity to control flow separation and induce mixing in microfluid devices designed in biomedical applications, such as magnetic drug carriers and lab-on-a-chip devices.
2. The Hall parameter proves to be a master switch to redirect flow. Raising m from 0.5 to 5.0 weakens electromagnetic braking on the primary flow by 35% and accelerates transverse flow speeds by a factor of 400%. The large sensitivity highlights the potential use of the Hall effect in non-invasive flow redirection techniques in physiological conditions particularly in targeted therapies, in which transversal flow determines the deposition of particles.
3. Though with different origins, ion-slip phenomena are seen to complement Hall currents by further weakening Lorentz damping in addition to offering more modest control over secondary transport phenomena. The subtle variation offers an extra degree of freedom to fine-tune electromagnetic flow control with greater accuracy in strongly driven regimes.
4. The resistance in the porous medium represented by $invDa$ constitutes a prominent regulating mechanism with regards to flow topology, such that greater resistance inhibits axial flow strongly and promotes lateral flow instead. The above-mentioned application is particularly pertinent to the delivery of drugs within the porous medium that constitutes tumors and/or the inflamed endothelium.
5. Buoyancy forces due to thermal and solutal gradients mainly drive the mean flow with negligible effect on the secondary flow; this implies that natural convection can be appropriately exploited to facilitate the advection of nutrients and drugs in the axial direction without affecting the secondary mixing pattern.

Taken together, these results go beyond incremental modeling to provide the physically interpretable toolbox that engineers and medical professionals need to design biomedical interventions with unprece dented specifi city using MHD parameters as design knobs that are more than mere dimensionless numbers.

5.9 Biomedical Applications and Implications

The results that are derived from this research are useful beyond the theoretical realms of fluid dynamics they can be applied to various biomedical areas such as

- **Surgical Techniques:** In critical surgical procedures such as neurosurgery, cardiovascular intervention, and microvascular treatment blood flow regulation is an essential criterion to prevent blood loss with adequate perfusion. The results show that the use of the external magnetic field can modulate blood flow without invading the surgical bleeding.
- **Magnetic Drug Delivery:** The Hartmann number and Hall parameter could be varied to allow precise guidance of therapeutic drugs. In fact, the increase in secondary flow saturation with higher Hall parameters m will lead to increased lateral dispersivity and making them more ideal for uniform therapeutic dispersivity in tortuous vasculature such as that found in tumors.
- **Hyperthermia Treatment:** The significant Joule heating effect with higher Hartmann numbers offers a quantitative basis for optimizing thermal dosing in

cancer treatments. It becomes possible to increase the temperature locally to the extent that it is sufficient to destroy cancerous areas without affecting the surrounding normal regions sensitive equilibrium

- **Implantable Devices:** The principles that come out of our resistivity analysis might be applied to designing more sophisticated drug-eluting stents and other implantable devices. The key would be to implement porosity and electromagnetic sensitivity to functionally release drugs depending on hemodynamic factors.
- **Sophisticated Diagnostics:** The magnetic field influences blood velocity and thermal distributions in subtle but discernable ways that need to be taken into consideration during hemodynamic analysis with the MRI. Additionally, these phenomena might form the basis of new contrast techniques or imaging markers for the detection of vascular dysfunction.

In other words, the research contains numerous applications that connect fundamental physics principles to practical applications in bio-medical engineering to ensure safer surgery and more intelligent drug delivery systems.

6 Conclusion

The present study provides a holistic and physics-informed analysis of unsteady blood flow with complex coupling among magnetic fields, Hall currents, ion slip effects, porous media, and joint thermal- buoyancy forces in the stretching blood vessel. A practical problem setup that is substantially pertinent to biomedical applications. The present problem is solved with substantial numerical rigor by transforming the set of partial differential equations to those involving ordinary differential equations with the help of similarity variables and then solved by bvp4c solver in MATLAB. The modeling procedure is firmly grounded in rigorous validation with best-known benchmark solutions and supported by extensive sensitivity analysis with respect to significant dimensionless parameters. The outcome goes beyond the enhancement of fundamental insight into MHD biofluid dynamics and provides practical expertise essential in real-world applications ranging from magnetic drug targeting and hyperthermia treatments to the development of intelligent vascular implants. In this manner, the present study aims to connect fundamental modeling with practical biomedical engineering.

7 Nomenclature

Roman Symbols

B_0	Magnetic field strength (T)
C	Concentration (mol/m^3)
C_f	Skin friction coefficient
C_p	Specific heat at constant pressure (J/kgK)
D	Mass diffusivity (m^2/s)
Da	Darcy number
Ec	Eckert number
f	Dimensionless stream function
g	Gravitational acceleration (m/s^2)
g	Dimensionless secondary velocity
Gr	Grashof number
Ha	Hartmann number
k	Thermal conductivity (W/mK)
k_1	Chemical reaction rate (1/s)
K	Permeability of porous medium (m^2)
L	Characteristic length (m)
m	Hall parameter
N	Velocity slip parameter
Nu	Nusselt number
Pr	Prandtl number
Re	Reynolds number
s	Ion-slip parameter
Sc	Schmidt number
Sh	Sherwood number
T	Temperature (K)
u, v, w	Velocity components (m/s)
x, y, z	Cartesian coordinates (m)

Greek Symbols

β_C	Solutal expansion coefficient (1/mol)
β_T	Thermal expansion coefficient (1/K)
γ	Chemical reaction parameter
η	Similarity variable
θ	Dimensionless temperature
κ	Thermal conductivity (W/mK)
λ_C	Solutal buoyancy parameter
λ_T	Thermal buoyancy parameter
μ	Dynamic viscosity (Pas)
ν	Kinematic viscosity (m^2/s)
ρ	Density (kg/m^3)
σ	Electrical conductivity (S/m)
ϕ	Dimensionless concentration
ω_e	Electron cyclotron frequency (rad/s)
τ_e	Electron collision time (s)
τ_w	Wall shear stress (Pa)
Δ	Combined Hall and ion-slip parameter $(1+$
Λ	Energy equation parameter $((1+s)^2+m^2)$

Subscripts

w	Condition at the wall
∞	Free stream condition
0	Reference condition
x	Local condition in x-direction
T	Thermal property

C	Solutal property
Dimensionless Parameters	
f_w	Suction/injection parameter
g_w	Wall secondary velocity parameter
$invDa$	Inverse Darcy number (ν/aK)
Mathematical Operators	
$'$	Differentiation with respect to η
∇	Gradient operator
∂	Partial derivative
∞	Infinity

REFERENCES

(1) Abbas, M. A. (2022). Analysis of entropy generation in magnetohydrodynamic (micropolar/Casson) flows over stretching surfaces. *Energies*, 15(3), 1206. https://doi.org/10.3390/en15031206

(2) Abo-Dahab, S. M., Mohamed, R. A., Abd-Alla, A. M., Soliman, M. S. (2023). Double-diffusive peristaltic MHD Sisko nanofluid flow through a porous medium in presence of non-linear thermal radiation, heat generation/absorption, and Joule heating. *Scientific Reports*, 13, Article 1432. https://doi.org/10.1038/s41598-023-27818-7

(3) Abubakar, J. U., Adeoye, A. D. (2020). Effects of radiative heat and magnetic field on blood flow in an inclined tapered stenosed porous artery. *Journal of Taibah University for Science*, 14(1), 7786. https://doi.org/10.1080/16583655.2019.1701397

(4) Abubakar, J. U., Omolesho, Q. A., Bello, K. A., Basambo, A. M. (2022). Casson rheological flow model in an inclined stenosed artery with non-Darcian porous medium and quadratic thermal convection. *Journal of the Egyptian Mathematical Society*, 30, Article 23. https://doi.org/10.1186/s42787-022-00157-8

(5) Ahmad, J., Siddiqui, B. K., Hassan, Q. M. U., Ali, R. (2024). Modeling blood flow in a stenotic artery using Maxwell Au-blood nanofluid: Insights into hemodynamics and nanoparticle dispersion. *BioNanoScience*, 14, 110. https://doi.org/10.1007/s12668-023-01232-9

(6) Alam, J., Murtaza, M. G. (2024). Significance of biomagnetic fluid flow with Ni-ZnFeO particle over a wedge in the presence of a magnetic dipole. *Multiscale and Multidisciplinary Modeling, Experiments and Design*, 7, 56735684. https://doi.org/10.1007/s41939-024-00526-z

(7) Anderson, H. I. (1992). MHD flow of a viscoelastic fluid past a stretching surface. *Acta Mechanica*, 95(14), 227230. https://doi.org/10.1007/BF01170814.

(8) Davidson, P. A. (2001). An introduction to magnetohydrodynamics. Cambridge University Press.

(9) Das, S., Barman, B., Jana, R. N., Makinde, O. D. (2021). Hall and ion slip currents' impact on electromagnetic blood flow conveying hybrid nanoparticles through an endoscope with peristaltic waves. *(*BioNanoScience, 11, 770792. https://doi.org/10.1007/s12668-021-00873-y

(10) Global Burden of Disease Collaborative Network. (2023). Global Burden of Disease cardiovascular burden estimates 19902022. Institute for Health Metrics and Evaluation. https://doi.org/10.6069/pyg4-me78

(11) Hammed, F. A., Usman, M. A., Akanbi, O. O. (2024). Irreversibility analysis of Hall effect on hydromagnetic blood flow in an inclined stretching permeable vessel.

IAENG International Journal of Applied Mathematics, 54(11), 22352252.

(12) Imoro, I., Etwire, C. J., Musah, R. (2024). MHD flow of a blood-based hybrid nanofluid through a stenosed artery with thermal radiation effect. *(*Case Studies in Thermal Engineering, 59, Article 104418. https://doi.org/10.1016/j.csite.2024.104418

(13) Kenjeres, S., Tjin, J. L. (2017). Numerical simulations of targeted delivery of magnetic drug aerosols in the human upper and central respiratory system. *Royal Society Open Science*, 4(12), 170873. https://doi.org/10.1098/rsos.170873

(14) Khanduri, U., Sharma, B. K. (2023). Mathematical analysis of Hall effect and hematocrit-dependent viscosity on Au/GO-blood hybrid nanofluid flow through a stenosed catheterized artery with thrombosis. *Advances in mathematical modelling, applied analysis and computation* (pp. 145167). Springer.

(15) Kierzenka, J., Shampine, L. F. (2001). A BVP solver based on residual control and the MATLAB PSE. *ACM Transactions on Mathematical Software*, 27(3), 299316.

(16) Krishna, M. V., Chamkha, A. J. (2020). Hall and ion slip effects on unsteady MHD convective rotating flow of nanofluidsApplication in biomedical engineering. *Journal of the Egyptian Mathematical Society*, 28(1), 1. https://doi.org/10.1186/s42787-019-0065-2

(17) Krishna, M. Veera, Bharathi, K., Chamkha, A. J. (2018). Hall effects on MHD peristaltic flow of Jeffrey fluid through porous medium in a vertical stratum. *Interfacial Phenomena and Heat Transfer*, 6(3). https://doi.org/10.1615/InterfacPhenomHeatTransfer.2019030215

(18) Mabood, F., Khan, W. A., Ismail, A. I. M. (2020). Analysis of MHD blood flow with thermal radiation. *Computer Methods and Programs in Biomedicine*, 188, 105296. https://doi.org/10.1016/j.cmpb.2020.105296

(19) Misra, J. C., Sinha, A. (2013). Effect of thermal radiation on MHD flow of blood and heat transfer in a permeable capillary in stretching motion. *Heat and Mass Transfer*, 49, 617628.

(20) Mishra, N. K. (2024). Computer simulation of heat and mass transfer effects on nanofluid flow of blood through an inclined stenosed artery with Hall effect. *Acta Mechanica et Automatica*, 18(1), 129138. https://doi.org/10.2478/ama-2024-0017

(21) Mohamed, A., Yasser, A., Taous, K. (2022). Human hypertension blood flow model using fractional calculus. *Frontiers in Physiology*, 13, 838593.

(22) Nadeem, S., Maraj, E. N., Akbar, N. S. (2014). Investigation of peristaltic flow of Williamson nanofluid in a curved channel with complaint walls. *Applied Nanoscience*, 4(5), 511-521. https://doi.org/10.1007/s13204-013-0234-9

(23) Nield, D. A., Bejan, A. (2006). Convection in porous media (3rd ed.). Springer.

(24) Priya, G. H., Vijaya, R. B., Prasad, R. S. (2015). Hall current effects on steady hydromagnetic rotating flow of a viscous incompressible fluid through a porous medium in a parallel plate channel with radiative heat transfer. *Quest Journals Journal of Research in Applied Mathematics*, 2(2), 111.

(25) Reddy, K. S. N., Babu, M. S., Varma, S. V. K., Reddy, N. B. (2014). Hall current and Dufour effects on MHD flow of a micropolar fluid past a vertical plate in the presence of radiation absorption and chemical reaction. *IOSR Journal of Mathematics*, 10(4), 106121

(26) Rekha, B., Usha, A. (2011). Mathematical model of blood flow in small blood vessel in the presence of a magnetic field. *Applied Mathematics*, 2, 264269.

(27) Sharma, B. K., Gandhi, R. (2023). Entropy-driven optimization of radiative Jeffrey tetrahybrid nanofluid flow through a stenosed bifurcated artery with Hall effects. *Physics of Fluids*, 35(12), 121903. https://doi.org/10.1063/5.0178352

(28) Shaw, S., Mahanta, G. (2021). Chemical reaction effects on MHD bio-convective flow. *Applied Mathematics and Computation*, 390, 125618.

(29) Sutton, G. W., Sherman, A. (1965). Engineering magnetohydrodynamics. McGraw-Hill.

(30) Tyagi, M., Zainal, N. A. (2025). Magneto nanofluid dynamics in a cosine-shaped stenosed artery: A finite difference approach. *JP Journal of Heat and Mass Transfer*, 38(2), 253265. https://doi.org/10.17654/0973576325012

(31) Vanguard Nigeria. (2023, September 28). Cardiovascular diseases responsible for 11% of NCD deaths in Nigeria. Vanguard News. https://www.vanguardngr.com/2023/09/cardiovascular-diseases-responsible-for-11-ncd-deaths-in-nigeria-minister/

(32) Veera Krishna, M., Chamkha, A. J. (2019). Hall and ion slip effects on MHD rotating boundary layer flow of nanofluid past an infinite vertical plate embedded in a porous medium. *Results in Physics*, 15, 102652. https://doi.org/10.1016/j.rinp.2019.102652

(33) Veera Krishna, M. V., Chamkha, A. J. (2020). Hall and ion slip effects on unsteady MHD convective rotating flow of nanofluidsApplication in biomedical engineering. *Journal of the Egyptian Mathematical Society*, 28, Article 1.

(34) Visweswara, S., Palani, B., Al Mukahal, F. H. H., Raju, S. S. K., Souayeh, B., Varma, S. V. (2025). Thermal entropy generation in magnetized radiative flow through porous media over a stretching cylinder. *Mathematics*, 13(19), 3189. https://doi.org/10.3390/math13193189

(35) Wahab, H. A., Shah, S. A. A., Ghafari, A. (2022). Computational analysis of MHD blood flow through a stenosed artery. *Journal of Biomechanical Engineering*, 144(3), 031004.

(36) World Health Organization. (2023). Nigeria: Age-standardized mortality rates for cardiovascular diseases and other NCDs. WHO Regional Office for Africa.

(37) World Health Organization. (2024). Global cardiovascular disease mortality trends. World Health Organization. https://www.who.int/data/publications/cardiovascular-disease-2024

(38) Yamamoto, H., Saito, T., Tanaka, Y. (2023). Characteristics of blood flow velocity in the radial artery and finger measured using a clip-type pulsimeter with a Hall element. *AIP Advances*, 14(2), 025009. https://doi.org/10.1063/5.0134567

(39) Yasin, M., Hina, S., Naz, R. (2024). Influence of Hall and slip on MHD ReinerRivlin blood flow through a porous medium in a cylindrical tube. *Soft Computing*, 28, 27992810. https://doi.org/10.1007/s00500-023-09538-2

(40) Yousef, H., Vinay, P., Ching Jen, C. (2001). Apparent viscosity of human blood in a high static magnetic field. *Journal of Magnetism and Magnetic Materials*, 225(12), 180186. https://doi.org/10.1016/S0304-8853(00)01249-X